ORAL/POSTER REFERENCE: ICF100983OR

FATIGUE CRACK GROWTH WITH TENSILE RESIDUAL STRESSES

Y Prawoto[1] and RA Winholtz[1, 2]

[1]Department of Mechanical and Aerospace Engineering, University of Missouri
[2]Research Reactor Center, University of Missouri

ABSTRACT

Cracks were grown in specimens with and without initial residual stresses under conditions of constant applied stress intensity factor. The specimens with initial tensile residual stresses showed acceleration of the crack propagation rates. The residual stresses were converted to stress intensity factors using the weight function and added to the applied stress intensity factors using the superposition principle. The plastic zone size was also measured utilizing diffraction line broadening and a small synchrotron x-ray beam. The results show that the weight function method, combined with the three-component model of crack growth, provides a good prediction of fatigue crack propagation rates in tensile residual stress fields.

KEYWORDS

Residual stress, fatigue crack propagation, weight function, plastic zone, x-ray

INTRODUCTION

Previous studies [1-5] have found that residual stresses can increase or decrease fatigue resistance. The Paris model predicts crack growth rate as a power function of the stress intensity factor (SIF) range, but cannot predict any influence of residual stresses on crack growth rate. The Walker [6] model includes an effect of load ratio, $R = K_{min}/K_{max}$, which is affected by residual stresses. The Walker equation may be written as shown in Table 1, where da/dN is the crack growth rate, ΔK is the SIF range, and γ is the Walker exponent, which captures the R dependence. This model only captures the Stage II crack growth regime. Later models also include crack growth in Stages I and III [7,8]. The three-component (TC) model of Saxena [7] was used in this study and is also given in Table 1.

The weight function method provides a powerful and simple means for calculating SIFs from the residual stresses. The SIF at any future crack length, a, is computed from the residual stress distribution, $\sigma(x)$, on the prospective crack line using the relation [9-11]

$$K_R = \int_0^a \sigma(x) \cdot m(a,x) dx \,. \tag{1}$$

Here the weight function, $m(a,x)$, depends only on the geometry of the component. A number of studies using the weight function have been conducted [12-19].

TABLE 1
FATIGUE CHARACTERIZATION RESULTS

Model	Equation	Constants*
Walker	$\frac{da}{dN} = C\left[\frac{\Delta K}{(1-R)^{(1-\gamma)}}\right]^n$	$C = 2.4\times10^{-10}$ $N = 4$ $\gamma = 0.8$
Three-Component	$\frac{1}{(da/dN)} = \frac{A_1(R)}{(\Delta K)^{n_1}} + A_2(R)\left[\frac{1}{(\Delta K)^{n_2}} - \frac{1}{(K_c(1-R))^{n_2}}\right]$ where $A_1(R) = C_1(1-R)^{\alpha}$ for $0.1 \le R \le 0.5$ $A_1(R) = C_2$ for $0.5 \le R \le 0.8$ $A_2(R) = C_3(1-R)^{\beta}$	$C_1 = 1.6\times10^{18}$ $C_2 = 1.5\times10^{12}$ $C_3 = 4\times10^{9}$ $\alpha = 20$ $\beta = 0.5$ $n_1 = 10.5$ $n_2 = 4$ $K_c = 83$

*The constants relate da/dN and ΔK when their units are in [mm/cycle] and [MPa$\sqrt{}$m], respectively.

EXPERIMENTAL PROCEDURES

Material and Specimen Preparation

Hot-rolled 1080 steel plate (12.7 mm thick) was austenitized for 30 minutes at 800 °C followed by a water quench and tempering at 700 °C for 3 hours. The average ferrite grain and cementite particle sizes were 5.6 μm and 1 μm, respectively. Electro-polishing was used to remove 0.5 mm from the surfaces, without introducing residual stresses, for accurate x-ray diffraction measurements. The specimens were machined into compact tension (CT) specimens [20]. Tapered interference pins (20.8 mm/m) were inserted in tapered holes in half the specimens along the future crack plane, as shown in Figure 1. In the other half of the specimens, no pin was inserted and no hole was drilled. An interference level between the specimen and pin of 0.125 mm was achieved by pressing the pin into the specimen.

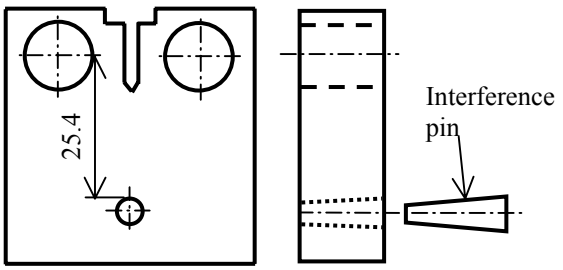

Figure 1: CT specimen with interference pin.

Initial Residual Stress Measurements

The initial residual stresses were measured using x-ray diffraction [21]. A chromium rotating anode source was used with x-rays of wavelength 2.2897 Å. A tapered glass capillary tube was used to focus the x-rays to a 210 μm spot. The stress component perpendicular to the future crack faces was measured along the prospective crack line.

Fatigue Crack Propagation Measurements

Fatigue cracking was performed under software control [22] using a sinusoidal waveform at 4 Hz. The crack length was measured using the compliance method [20] and was also monitored using a traveling microscope. First, the material constants for the Walker and TC models given in Table 1 were determined with residual stress free specimens. Next, two specimens were cracked at each of six different constant ΔK values, ranging from 17.5 to 25 MPa$\sqrt{m}$, one with and one without residual stresses, all with an applied load ratio of R=0.1.

Plastic Zone Size Measurements

The size of the plastic zone was determined from line broadening of the diffraction peaks using a 50 x 50 μm synchrotron x-ray beam. The method relies on the broadening of a diffraction peak with plastic deformation due to an increased dislocation density. The specimens were sectioned longitudinally to obtain the interior plastic zone size. The sectioned surface was metallographically polished and etched to remove the damage from sectioning. Experiments were performed at the SRI CAT 1-BM beamline at the Advanced Photon Source, Argonne National Laboratory. X-rays of 10 keV were used and the Fe-411 peak was studied. The crack surface was found by monitoring the iron fluorescence produced by the x-ray beam. The line broadening was monitored as the beam moved into the interior of the specimen perpendicular to the crack face. This procedure was repeated at a number of positions along the crack line to determine the plastic zone size as the crack grew through the specimen.

RESULTS AND ANALYSIS

Residual Stress Intensity Factor

Figure 2 shows the initial residual stresses on the specimen before fatigue cracking along the prospective crack line on both the front and back faces of the specimen. Near the pin interface, there are some differences between the front and back faces due to friction while inserting the pin. Finite element modeling of the insertion process gives comparable results for the faces and shows that the stress distribution in the interior of the specimen is similar [23]. The average of the front and back faces was used in further analysis. The residual stresses were converted to a residual SIF using the weight function for a CT specimen [11] and Eqn. 1. Figure 3 shows the result of these calculations.

Crack Growth Rates

Predictions of the crack growth rates were made as follows. Using the superposition principle, the effective load ratio was calculated as

$$R' = \frac{K_{\min} + K_R}{K_{\max} + K_R}. \tag{4}$$

The effective load ratio, R', changes from the original applied load ratio. Here, $K_{\min}$ and $K_{\max}$ are the minimum and maximum applied SIFs, and K_R is the residual SIF shown in Figure 3. Having calculated R', shown in Figure 4, the da/dN predictions were then made using the constants in Table 1. Figure 5 shows experimental and predicted crack growth rates for a specimen containing residual stresses loaded with a constant applied ΔK. The predictions based on the TC model fit best with the experiment results. Results for five other specimens, loaded at different ΔK values, show similar trends.

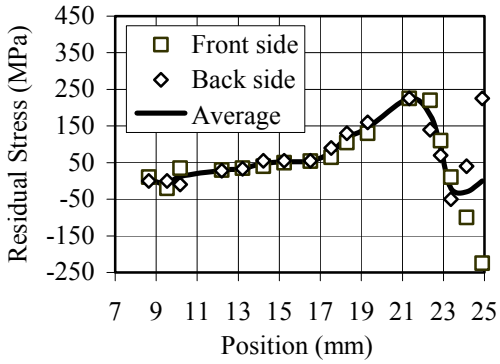

Figure 2: Initial tangential residual stress along the prospective crack line.

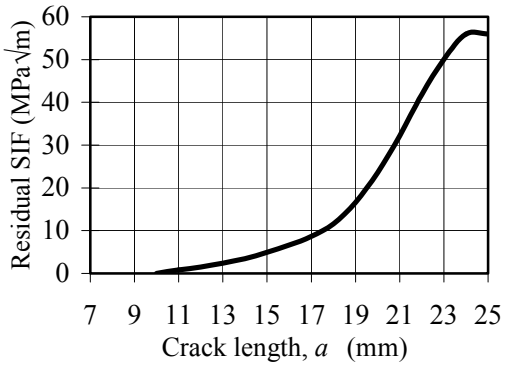

Figure 3: Residual SIF calculated using the weight function.

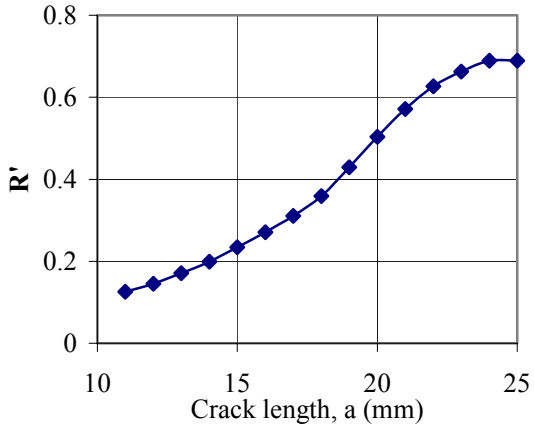

Figure 4: (a) Effective load ratio, R', as a function of crack length for residual stress specimens.

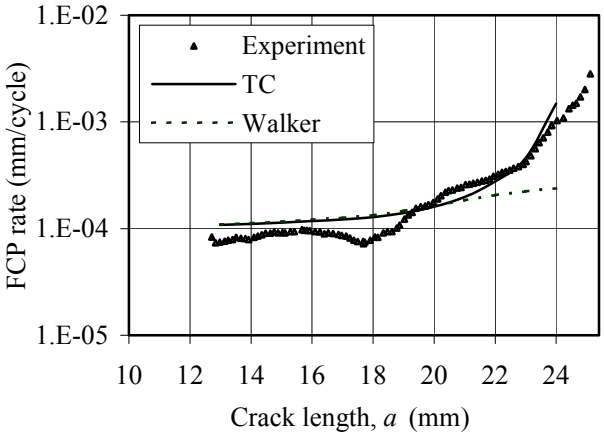

Figure 5: Comparison of predicted and experimental crack growth rates with Constant applied SIF range ΔK=25 MPa√m.

Plastic Zone Measurements

Experimental determination of the plastic zone size along the crack line is shown in Figure 6. Even though the specimen experienced a constant maximum applied SIF of 25 MPa√m, the plastic zone size was found to increase as the crack entered the residual stress field.

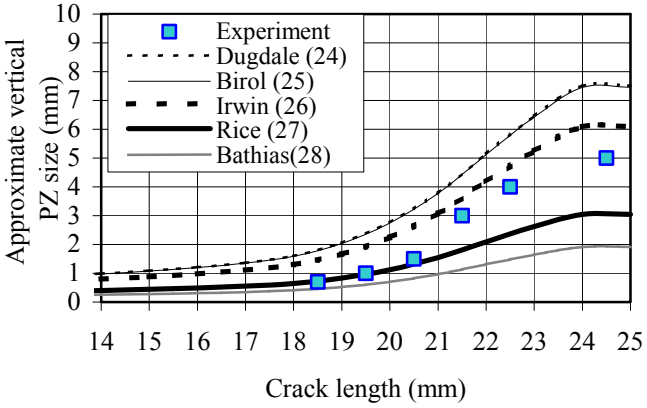

Figure 6: Vertical plastic zone sizes in the interior of the sample. Note the Dugdale and Birol solutions are nearly overlapped.

The results here are also compared with some analytical and experimental approximations available [24-28]. The predictions in the figures were made by assuming that the total maximum SIF is the superposition of the maximum applied SIF and the residual SIF. The experimental results obtained here fall in between the Rice and Irwin analytical solutions [26,27]. The experimental results are also shown compared to calculations based on constants experimentally obtained by Birol [25], which was based on an etching method, and Bathias [28], which was based on a microhardness method.

SUMMARY AND CONCLUSIONS

Accurate predictions of fatigue crack growth rates through residual stress fields were obtained from the superposition of residual stresses and applied stresses using the weight function approach. Both the residual stresses and the applied stresses were converted to stress intensity factors independently and then combined using the basic principle of linear elastic superposition. The specimens with initial tensile residual stresses show acceleration of the crack propagation rates, which compare well with predictions based on models. Evaluation of the results lead to the following conclusions:

1. The residual stresses in a specimen can be used, with the weight function, to compute a residual stress intensity factor that a crack will experience as it propagates through the residual stresses. Then, with a crack propagation law, one can predict the fatigue crack growth rate of a crack growing into a tensile residual stress field. Superposition may not work satisfactorily if either the residual or applied stress intensity factors are compressive. If the net stress intensity factor is decreasing as the crack grows, the plastic zone size is decreasing which can cause the crack to behave differently than the growth model.

2. Tensile residual stresses accelerate a fatigue crack by increasing the load ratio. This has two effects. First, materials display a load ratio sensitivity, usually quantified by the Walker exponent γ, such that cracks grow faster at a higher load ratio. Secondly, at a higher load ratio cracks will transition into the more rapid Stage III growth regime at a lower stress intensity range. This effect can be seen in Figure 5 as the point where the TC model deviates from the Walker model predicting higher crack growth rates and better representing the experimental data.

3. The three-component model of Saxena gives a good prediction of fatigue crack propagation rates when used with the superposition of the applied and residual stress intensity factors. It captures both of the load ratio sensitivity and the transition to Stage III growth and hence makes a better prediction for the crack growth rate than the Walker model.

4. The size of the plastic zone can be measured with a small synchrotron x-ray beam along a fatigue crack by measuring the diffraction line broadening of the material perpendicular to the crack faces. The superposition of the residual stress intensity factor and the maximum applied stress intensity factor during fatigue crack growth correctly predicts the shape of the plastic zone size variation as a fatigue crack grows into a tensile residual stress field. The measured size of the plastic zone falls between the theoretical predictions of Rice and Irwin, which give upper and lower bounds, respectively.

ACKNOWLEDGEMENTS

The authors would like to acknowledge the University of Missouri Research Board for funding this research. They also express thanks to J.D. Almer and J.B. Cohen for performing the initial residual stress measurement at Northwestern University. The assistance of D.R. Haeffner and P.L. Lee with the synchrotron x-ray measurements is gratefully acknowledged. The use of the

Advanced Photon Source was supported by the U.S. Department of Energy, Basic Energy Sciences, Office of Science, under Contract No. W-31-109-Eng-38.

REFERENCES

1. Underwood, J.H, Pook, L.P. and Sharples, J.K. (1977) *ASTM STP 631,* 402.
2. Underwood, J.H. (1995) *Exp. Mech.* 35, 61.
3. Elber W., (1971) *ASTM STP 486*, 230.
4. Nelson, D.V. (1982) *ASTM STP 776*, 172.
5. Parker, A.P. (1982) *ASTM STP 776*, 13.
6. Walker, K. (1970) *ASTM STP 462*, 1.
7. Saxena, A., Hudak, S.J. Jr., and Jouris, G.M. (1979) *Eng. Fract. Mech.*, 12, 103.
8. Miller, M.S. and Gallagher, J.P. (1981) *ASTM STP 738*, 205.
9. Wu, X.R. (1984) *Eng. Fract. Mech*., 20, 35.
10. Wu, X.R. and Carlsson, A.J. (1991) *Weight Functions and Stress Intensity Factor Solutions*, Pergamon Press, Oxford.
11. Fett, T. and Munz, D. (1997) *Stress Intensity Factors and Weight Functions*, Computational mechanics publications, Southampton.
12. Stacey, A. and Webster, G.A. (1988) *ASTM STP 1004*, 37.
13. Nguyen, N. and Wahab, M.A. (1996) *Welding Journal*, 75, 55s.
14. Itoh, Y.Z. (1989) Eng. Fract. Mech., 33, 397.
15. Okamoto, A. and Nakamura, H. (1990) *J. Pressure Vessel Tech.,* 112, 199.
16. Glinka, G. (1979) *ASTM STP 677*, 198.
17. Glinka, G. (1987) *Advances in Surface Treatments: Technology-Applications-Effects*, Pergamon, 413.
18. Todoroki, A. and Kobayashi, H. (1988) *Trans. Japan Soc. Mech. Eng.,* A-54 30.
19. Todoroki, A. and Kobayashi, H. (1990) *Proceeding of the LSME/JSME Joint Conference*, Seoul, Korea, 367.
20. ASTM Standards, ASTM E 647-95a.
21. Almer, J.D., Cohen, J.B., and Winholtz, R.A. (1998) *Metall. and Matls. Trans*, 29A, 2127.
22. MTS Systems Corporation (1993) '*759.40 Testware fatigue crack growth test operator's guide'*, MTS System Corporation.
23. Almer, J.D., Cohen, J.B., McCallum, K.R., and Winholtz, R.A. (1997) *Proc. of the Fifth International Conference on Residual Stress*, Soc. Exp. Mech., Bethel, CT, 1072.
24. Dugdale, D.S. (1960) *J. of Mech. and Phys. of Solids*, 8, 100.
25. Birol, Y. (1988) *J. of Mater. Sci*, 23, 2079.
26. Irwin, G.R. (1960) *Proc. of Seventh Sagamore Ordnance Materials Conference*, Syracuse University, IV 63.
27. Rice, J.R. (1972) *Int. J. Solids Structures*, *8*, 751.
28. Bathias, C. and Pelloux, R.M. (1973) *Metall. Trans.*, 4, 1265.